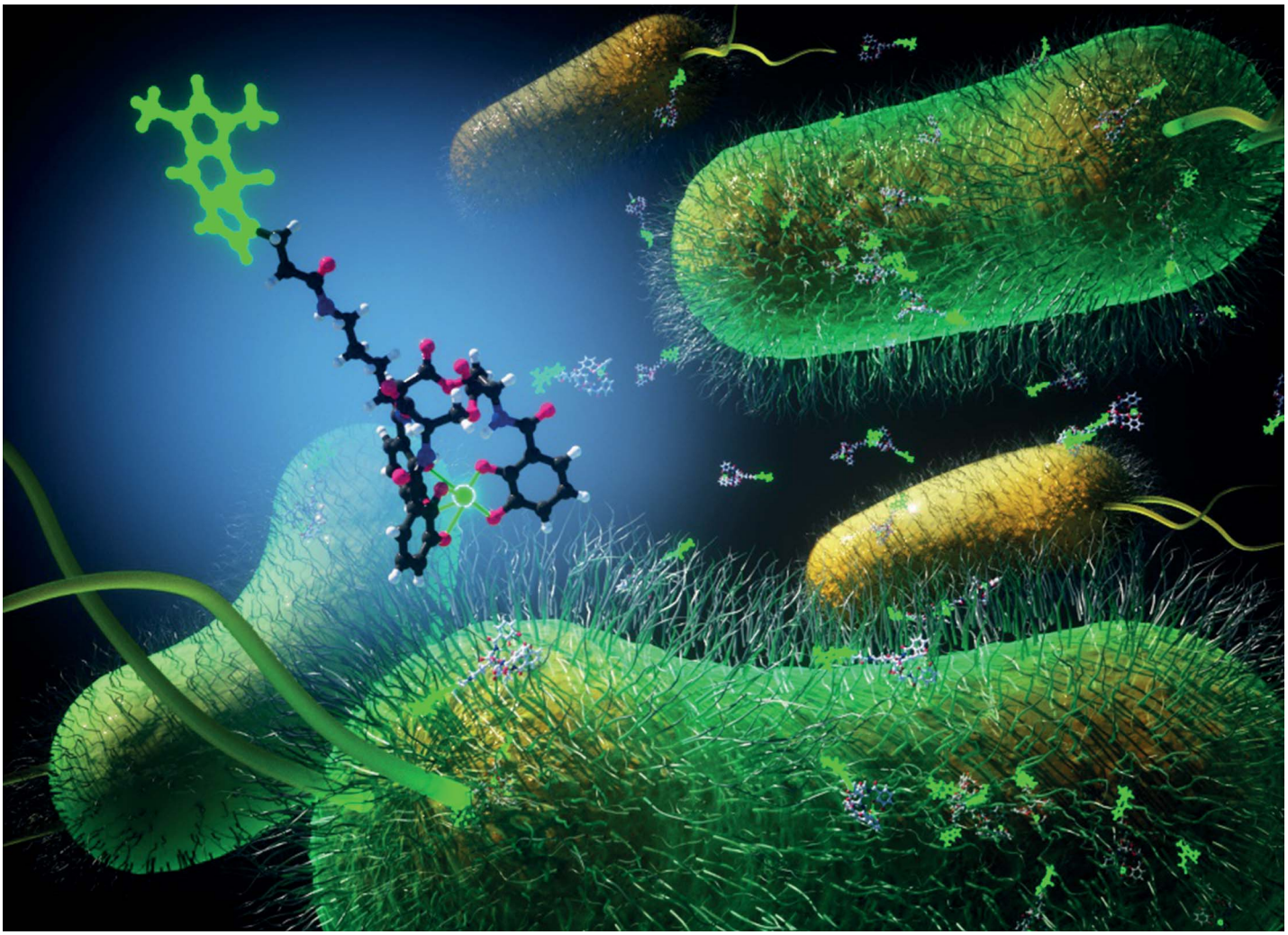

Showcasing research from the KlahnLab, Institute of Organic Chemistry, Technische Universität Braunschweig, Lower-Saxony, Germany.

Biomimetic enterobactin analogue mediates iron-uptake and cargo transport into *E. coli* and *P. aeruginosa*

The design, synthesis and biological evaluation of the artificial enterobactin analogue **Ent$_{KL}$** and several fluorophore-conjugates thereof are described. **Ent$_{KL}$** provides an attachment point for cargos such as fluorophores or antimicrobial payloads. Showing similar iron binding behaviour compared to the natural product, **Ent$_{KL}$** exhibited potent concentration-dependent growth promoting effects in siderophore biosynthesis deficient mutants of *E. coli* and *P. aeruginosa* and was demonstrated to be able to deliver fluorescent molecular cargos *via* the bacterial iron transport machinery into the bacteria.

The artwork was created by Ella Maru Studios and the copyright is held by Dr. Philipp Klahn.

As featured in:

See Philipp Klahn *et al.*, *Chem. Sci.*, 2021, **12**, 10179.

ROYAL SOCIETY OF CHEMISTRY

rsc.li/chemical-science

Registered charity number: 207890

Chemical Science

ROYAL SOCIETY OF CHEMISTRY

EDGE ARTICLE

View Article Online
View Journal | View Issue

Check for updates

Cite this: *Chem. Sci.*, 2021, **12**, 10179

All publication charges for this article have been paid for by the Royal Society of Chemistry

Open Access Article. Published on 17 June 2021. Downloaded on 10/3/2024 11:52:16 PM.
This article is licensed under a Creative Commons Attribution-NonCommercial 3.0 Unported Licence.

Biomimetic enterobactin analogue mediates iron-uptake and cargo transport into *E. coli* and *P. aeruginosa*†

Robert Zscherp,‡[a] Janetta Coetzee,‡[bc] Johannes Vornweg,[a] Jörg Grunenberg,[a] Jennifer Herrmann,[bc] Rolf Müller[bc] and Philipp Klahn *[a]

Received 14th April 2021
Accepted 16th June 2021

DOI: 10.1039/d1sc02084f

rsc.li/chemical-science

The design, synthesis and biological evaluation of the artificial enterobactin analogue Ent_{KL} and several fluorophore-conjugates thereof are described. Ent_{KL} provides an attachment point for cargos such as fluorophores or antimicrobial payloads. Corresponding conjugates are recognized by outer membrane siderophore receptors of Gram-negative pathogens and retain the natural hydrolyzability of the tris-lactone backbone. Initial density-functional theory (DFT) calculations of the free energies of solvation (ΔG(sol)) and relaxed Fe–O force constants of the corresponding $[Fe\text{-}Ent_{KL}]^{3-}$ complexes indicated a similar iron binding constant compared to natural enterobactin (**Ent**). The synthesis of Ent_{KL} was achieved *via* an iterative assembly based on a 3-hydroxylysine building block over 14 steps with an overall yield of 3%. A series of growth recovery assays under iron-limiting conditions with *Escherichia coli* and *Pseudomonas aeruginosa* mutant strains that are defective in natural siderophore synthesis revealed a potent concentration-dependent growth promoting effect of Ent_{KL} similar to natural **Ent**. Additionally, four cargo-conjugates differing in molecular size were able to restore growth of *E. coli* indicating an uptake into the cytosol. *P. aeruginosa* displayed a stronger uptake promiscuity as six different cargo-conjugates were found to restore growth under iron-limiting conditions. Imaging studies utilizing $BODIPY_{FL}$-conjugates, demonstrated the ability of Ent_{KL} to overcome the Gram-negative outer membrane permeability barrier and thus deliver molecular cargos *via* the bacterial iron transport machinery of *E. coli* and *P. aeruginosa*.

Introduction

The development of bacterial resistance towards antimicrobial drugs is an intrinsic part of bacterial evolution and this, in turn, necessitates the continuous development of novel drugs able to kill these life-threatening multi-drug resistant human pathogens.[1–3] Facing the current spread of bacterial resistance against clinically used antibiotics, the development of novel antimicrobial drugs and innovative concepts is of vast importance to counteract this serious threat for public health.[1,4,5]

Four of the six ESKAPE pathogens,[6,7] represent bacterial species considered as significant threat for public health due to a very high occurrence of multi-drug resistance, are Gram-negative bacteria. In addition, the pathogens recently prioritized by the WHO with a critical, high or medium need for the development of novel antimicrobial drugs are primarily Gram-negative bacteria, including β-lactam-resistant *Escherichia coli* and *Pseudomonas aeruginosa* or fluoroquinolone-resistant *Salmonella* and *Shigella* species.[8] However, the development of novel antimicrobial drugs against Gram-negative bacteria is challenging, not only due to the presence of drug exporters as also found in Gram-positive bacteria, but because many antibacterial compounds fail to overcome the Gram-negative outer membrane. As a consequence, many potential drugs displaying antibacterial activity against Gram-positive bacteria remain inactive against Gram-negative bacteria, although their biological targets are generally present, as they fail to translocate over the cell envelope barrier.[9]

An innovative approach to enable translocation of antimicrobial drugs or reporter molecules over the Gram-negative cell envelope barrier and to develop novel antimicrobial drugs against these pathogens is the conjugation and hybridization with siderophores.[4,10–12] Siderophores are small molecule iron chelators,[13,14] produced and secreted by bacteria, fungi and plants to ensure their supply with iron, an essential growth factor for all living organisms.[15] Beyond iron uptake,

[a]*Institute of Organic Chemistry, Technische Universität Braunschweig, Hagenring 30, D-38106 Braunschweig, Germany. E-mail: p.klahn@tu-bs.de*

[b]*Department for Microbial Natural Products, Helmholtz Institute for Pharmaceutical Research Saarland (HIPS), Helmholtz Center for Infection Research and Department of Pharmacy at Universität des Saarlandes, Campus Building E 8.1, D-66123 Saarbrücken, Germany*

[c]*German Center for Infection Research (DZIF), Site Hannover-Braunschweig, Germany*

† Electronic supplementary information (ESI) available. See DOI: 10.1039/d1sc02084f

‡ Authors contributed equally.

© 2021 The Author(s). Published by the Royal Society of Chemistry

Open Access Article. Published on 17 June 2021. Downloaded on 10/3/2024 11:52:16 PM.
This article is licensed under a Creative Commons Attribution-NonCommercial 3.0 Unported Licence.

siderophores have multiple other biological functions in bacteria,[16–18] *e.g.* they are important virulence factors contributing to pathogenesis.[17,19] After coordination of Fe(III), the resulting ferri-siderophores are recognized by specific siderophore receptors, transmembrane proteins embedded in the outer membrane, and are actively transported into the cytosol of bacteria.[4,20–23] Siderophore drug conjugates can enter bacterial cells *via* the same pathway through siderophore receptor mediated uptake.[1,4,24–32]

The general concept of this Trojan Horse approach is derived from natural antetypes. The sideromycins,[33] such as albomycins[34–36] or the microcins E492 (ref. 37–40) and H47 (ref. 41) are utilized by different bacteria to defend their ecological niche against competing bacteria. These natural siderophore drug conjugates reveal a remarkable increase in antibacterial activity compared to the parental free antibiotics. Inspired by this natural concept researchers have developed artificial siderophore drug conjugates based on synthetically modified siderophore analogues,[42–55] leading to active drug accumulation and tremendously increased antibacterial activity compared to the parental drugs.[42,43,48] Furthermore, siderophore drug conjugates can expand the activity of Gram-positive-only drugs towards Gram-negative pathogens.[50,51,56,57] Additionally, this strategy allows for the design of narrow-spectrum antibiotics,[10,49,57] selectively targeting specific virulent pathogens, thereby reducing the selection pressure on the bacterial resistome. Importantly, the siderophore-β-lactam hybrid cefiderocol developed by Shionogi Pharmaceuticals was recently approved by the FDA for the treatment of pneumonia caused by Gram-negative bacteria.[58]

In this context, the tris-catechol siderophore enterobactin (**Ent**, Scheme 1A)[14] displaying an extraordinarily high Fe(III) binding constant ($K_d = 10^{-49}$ M)[59,60] as well as its glycosylated derivatives, the salmochelins[61] evading lipocalin-2 inactivation,[62,63] are of high interest.

Ent and salmochelins are biosynthesized by Gram-negative bacteria of the family Enterobacteriaceae, such as *E. coli*, *Klebsiella pneumonia*, *Salmonella typhimurium*, *Yersinia enterocolitica* and *Shigella flexneri,* to ensure their iron supply.[64] However, **Ent** has also been found to be produced by Gram-positive *Streptomyces* species[65] and it serves as a xenosiderophore for the opportunistic human pathogen *P. aeruginosa*, where internalization is mediated by the outer membrane siderophore receptor PfeA.[66–69] **Ent** and salmochelins also play a crucial role during infection[18,70] and they have been demonstrated to sequester iron from human transferrin.[17,19] Previously reported artificial **Ent** analogues used for the development of siderophore drug conjugates or siderophore-based imaging tools[71,72] were based on modifications at one of the catechol units[42,43,46,49,52,73–75] or the natural tris-serine lactone backbone was substituted by artificial moieties to generate an attachment point for payloads in the backbone of the siderophore.[48,76–78] Although a co-crystal structure of $[\textbf{Fe-Ent}]^{3-}$ with its *E. coli* siderophore receptors of FepA[79,80] and IroN[80–82] is not available, recognition of $[\textbf{Fe-Ent}]^{3-}$ at other proteins such as FeuA,[83–85] VctP,[86] PfeA[69] or lipocalin-2 (ref. [83]) suggests that the attachment of larger payloads at the catechol units might interfere with $[\textbf{Fe-Ent}]^{3-}$ receptor recognition.

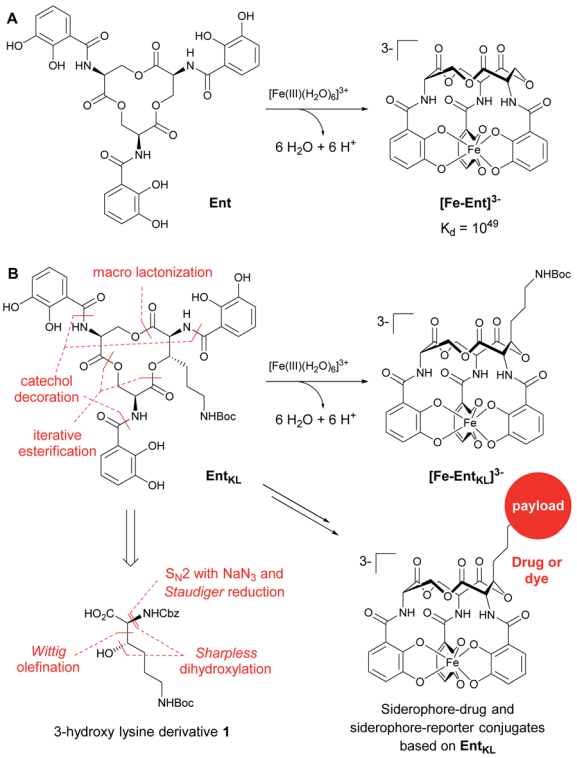

Scheme 1 (A) Structures of enterobactin (**Ent**) and ferri-enterobactin ($[\textbf{Fe-Ent}]^{3-}$); (B) retrosynthetic analysis and design concept of $\textbf{Ent}_{KL}$.

Therefore, we envisaged the synthesis of the novel, biomimetic enterobactin analogue $\textbf{Ent}_{KL}$ (Scheme 1B). Our synthesis is based on the incorporation of the 3-hydroxy lysine derivative **1** into **Ent** backbone, aiming to generate an attachment point for antimicrobial payloads in the backbone out of the recognition site of the siderophore and simultaneously retain the natural hydrolyzability of the tris-lactone backbone.[52,87]

Result and discussion

Retrosynthetically, the final siderophore could be derived from a modified asymmetric tris-lactone backbone by decoration with catechol units *via* amide coupling (Scheme 1B). As the tin-template mediated *trans*-esterification approach utilized earlier, by Shanzer,[88,89] later by Gutierrez[90] and Raymond[91] for the synthesis of the enterobactin tris-serine lactone backbone, leads exclusively to the formation of the thermodynamic, symmetric product, it is not applicable for the synthesis of the envisaged asymmetric tris-lactone backbone. Therefore, we decided to follow an approach of iterative assembly of a linear trimer containing the 3-hydroxy lysine derivative **1** with subsequent macro lactonization as used in the early synthesis of **Ent** by Corey,[92] Rastetter[93] and Rogers[94] in order to generate the desired asymmetric backbone of $\textbf{Ent}_{KL}$.

In order to estimate if the envisaged substituent at the asymmetric tris-lactone backbone would negatively impact the

© 2021 The Author(s). Published by the Royal Society of Chemistry

Open Access Article. Published on 17 June 2021. Downloaded on 10/3/2024 11:52:16 PM. This article is licensed under a Creative Commons Attribution-NonCommercial 3.0 Unported Licence.

solution thermodynamics and/or the kinetic stability of the Fe(III) complex $[\mathbf{Fe\text{-}Ent_{KL}}]^{3-}$, we computed the free energies of solvation ΔG(sol) as well as the relevant (relaxed) Fe–O force constants for $[\mathbf{Fe\text{-}Ent}]^{3-}$ and two stereoisomers of $[\mathbf{Fe\text{-}Ent_{KL}}]^{3-}$ bearing an axial or equatorial substituent (Table 1) following the protocol of Baramov *et al.*[95] (see ESI†).

In a first step, we tried to reproduce the experimentally well-known free energy of complexation (ΔG(sol): −66.8 kcal mol^{-1} (ref. 59 and 60)) for $[\mathbf{Fe\text{-}Ent}]^{3-}$.

Our calculated value of −64.5 kcal mol^{-1} for ΔG(sol) $[\mathbf{Fe\text{-}Ent}]^{3-}$ is very close to the literature ref. 59 and 60 positively validating our applied *in silico* procedure. Interestingly, the artificial ferri-enterobactin analogues seem to be even better iron binders than the unsubstituted $[\mathbf{Fe\text{-}Ent}]^{3-}$ by several kcal mol^{-1}. Furthermore, the value for $[\mathbf{Fe\text{-}Ent_{KL}(eq)}]^{3-}$ was calculated to be energetically more favored as compared to $[\mathbf{Fe\text{-}Ent_{KL}(ax)}]^{3-}$ by a value of 3.5 kcal mol^{-1}.

Nevertheless, the absolute values need to be considered with caution and we hypothesize that both artificial enterobactin analogues, $\mathbf{Ent_{KL}(eq)}$ and $\mathbf{Ent_{KL}(ax)}$, lead to complexes which are at least of similar thermodynamic stability compared to $[\mathbf{Fe\text{-}Ent}]^{3-}$ and that there is no significant energetical advantage of one analogue over the other. While siderophore Fe(III) complexes are thermodynamically very stable, they are kinetically labile. This is in contrast to, for example, their chromic counterparts, which are both thermodynamically and kinetically stable. In order to find out if this kinetic lability holds true also for our artificial ferri-enterobactin analogues, we calculated the relaxed Fe–O force constants, a method which was recently successfully applied in several other weakly bound systems. According to our computational results, all three complexes seem to be kinetically labile with relaxed Fe–O force constants well below 1 N cm^{-1} (see Table 1), indicating very weak bonds with less or no covalency.[96–100] (Note, that the averaged Cr–O value for $[\mathbf{CrEnt}]^{3-}$ is 1.25 N cm; unpublished results J. G.) Furthermore, our calculated Fe–O values are very similar. In summary, all three complexes seem to be kinetically labile, while being thermodynamically stable, as found earlier for $[\mathbf{Fe\text{-}Ent}]^{3-}$ by Raymond and co-workers.[101,102]

Thus, expecting no negative impact of an axial backbone substituent on the Fe(III) complex stability, we developed a robust, scalable synthetic route to the required 3-hydroxy lysine derivative **1** starting from commercially available 4-aminobutanol (**2**) as outlined in Scheme 2. A sequence of Boc protection, Swern oxidation of the resulting *N*-Boc-4-aminobutanol (**3**) to aminal **4** and final Wittig olefination in presence of methyl (triphenyl-phosphoranylidene) acetate (**5**) at 100 °C led to formation of the *E*-configured α,β-unsaturated methyl ester **6** in excellent diastereoselectivity of $E : Z = 100 : 1$ and 89% yield over 3 steps with only a single chromatographic purification step being required. An asymmetric sharpless dihydroxylation using AD-mix-α finally gave diol **7** in 83% yield. The formation of the corresponding cyclic sulfite in the presence of thionyl chloride and triethyl amine at 0 °C and subsequent α-inversion in the presence of sodium azide afforded α-azido methyl ester **8** in 64% yield. At this step the absolute

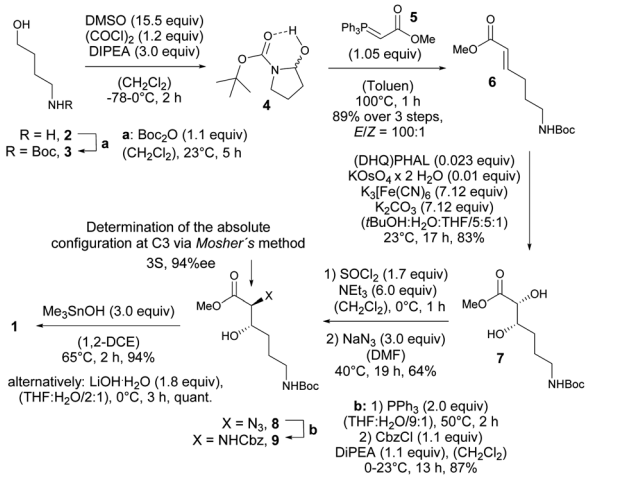

Scheme 2 Synthesis of 3-hydroxy lysine derivative **1**.

Table 1 Calculated ΔG(sol) and averaged, relaxed force constants of the Fe–O single bonds of $[\mathbf{Fe\text{-}Ent_{KL}}]^{3-}$, $[\mathbf{Fe\text{-}Ent_{KL}(ax)}]^{3-}$ and $[\mathbf{Fe\text{-}Ent_{KL}(eq)}]^{3-}$

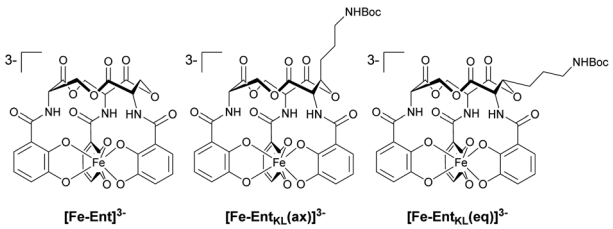

	$[\mathbf{Fe\text{-}Ent}]^{3-}$	$[\mathbf{Fe\text{-}Ent_{KL}(ax)}]^{3-}$	$[\mathbf{Fe\text{-}Ent_{KL}(eq)}]^{3-}$
ΔG(sol)^{a,b} [kcal mol^{-1}]	−64.5	−67.2	−70.7
ΔG(sol)^{a,b} [kJ mol^{-1}]	−269.9	−281.6	−296.0
Fe–O bond force constant (av)^{a} [N cm^{-1}]	0.95	0.97	0.98

^{a} Computed for DMSO as solvent. ^{b} Separate consideration of all hydronium ions.

Open Access Article. Published on 17 June 2021. Downloaded on 10/3/2024 11:52:16 PM.
This article is licensed under a Creative Commons Attribution-NonCommercial 3.0 Unported Licence.

configuration at the C3 position introduced by the sharpless dihydroxylation was determined to be S-configured with an enantiomeric excess of 94%ee using Mosher's method.[103]

Finally, a Staudinger reduction and subsequent Cbz protection generated the methyl ester **9** in 87% yield, which was saponified in the presence of trimethyltin hydroxide in 1,2-dichloro ethane at 65 °C using Nicolaou's protocol[104] yielding the desired 3-hydroxy lysine derivative **1** in 94%.

With **1** in hands, we achieved the assembly of the linear trimer **17** as outlined in Scheme 3. First, the 2-methylanthraquinyl ester **11** was formed with 2-bromomethylanthraquinone **10** (MaqBr) in the presence of DBU in 55% yield.[93] A two times consecutive sequence of Steglich esterification with Cbz-Ser(TBS)-OH **12** and subsequent desilylation in the presence of a mixture of aqueous, concentrated HF solution and TBAF led to the Maq-protected linear trimer **16** obtained in 64% yield over 4 steps. Ester **16** was then photolytically cleaved at 360 nm in the presence of *N*-methyl morpholine (NMM) in a mixture of iso-propanol and chloroform giving the unprotected linear trimer **17** as precursor for the backbone cyclization in 65% yield.[93]

As expected for the formation of a 12-membered ring with several axial substituents, the cyclization of **17** to the tris-lactone **18** was challenging.

The activation of the carboxylic acid *via* several reagents predominantly led to elimination under formation of the corresponding dihydro amino acid (Table 2).

After extensive screening of different methods for the macro lactonization, a first success with a low yield of 13% was achieved using Shiina's reagent[105] (Entry 1, Table 2). Any other screened coupling reagent such as different carbodiimides, PyBOP, T_3P (propylphosphonic anhydride) or Yamaguchi's reagent[106] could not furnish the macro lactonization, favouring elimination. The activation of the alcohol through intramolecular Mitsunobu reaction gave similarly a low yield of 14% (Entry 2, Table 2). Finally, the highest yield of 50% for tris-lacton **18** was obtained using Gerlach's modification[107] of the Corey–Nicolaou macro lactonization,[108] first formation of the intermediate thioester using Corey's disulfane and subsequent silver-catalyzed cyclization at 23 °C in benzene (Entry 3, Table 2).

However, as the yield of this reaction was hardly reproducible, we finally applied 2,2′-dipyridyldisulfide to form the intermediate thioester and furnished macro lactonization in the presence of silver acetate giving 32% yield of the desired tris-lactone **18** reliably (Entry 4, Table 2).

The final quantitative, hydrogenolytic Cbz deprotection required 20 atm of hydrogen gas in a mixture of methanol, ethyl acetate and TFA. Subsequent acylation under Schotten–Baumann conditions with 2,3-diacetoxybenzoic acid chloride **19** or 2,3-dimethoxybenzoic acid chloride **20**, respectively, led to the formation of **(AcO)Ent$_{KL}$** and **(MeO)Ent$_{KL}$**. **Ent$_{KL}$** could be obtained in low yield from **(AcO)Ent$_{KL}$** by mild saponification in diluted methanolic ammonia.

However, as it has been reported that acetylated siderophore-prodrugs can be activated *in situ* and are favorable to prevent the inactivation of catecholates by enzymatic methylation,[48,76,109,110] we employed **(AcO)Ent$_{KL}$** as siderophore-prodrug and **(MeO)Ent$_{KL}$** as starting point for the synthesis of corresponding negative control probes, unable to bind iron or mediate uptake in our approach. In order to determine if the synthesized enterobactin derivatives are internalized by *E. coli* and *P. aeruginosa* during iron limitation, growth recovery assays were done with mutant strains that lack the ability to biosynthesize siderophores, and therefore require external siderophores to be able to grow under iron-limiting conditions. Importantly, iron-limiting conditions are typically found *in vivo* at the site of infections being part of the host immune response to prevent bacterial growth.[58,111,112] *E. coli* K-12 Δ*entA* grew to $OD_{600} \approx 0.35$ in 50% MHB II medium (37 °C, $t = 24$ h), and this value decreased to <0.05 when 200 μM 2,2′-bipyridine (DP) was added to the media in order to simulate iron-limiting

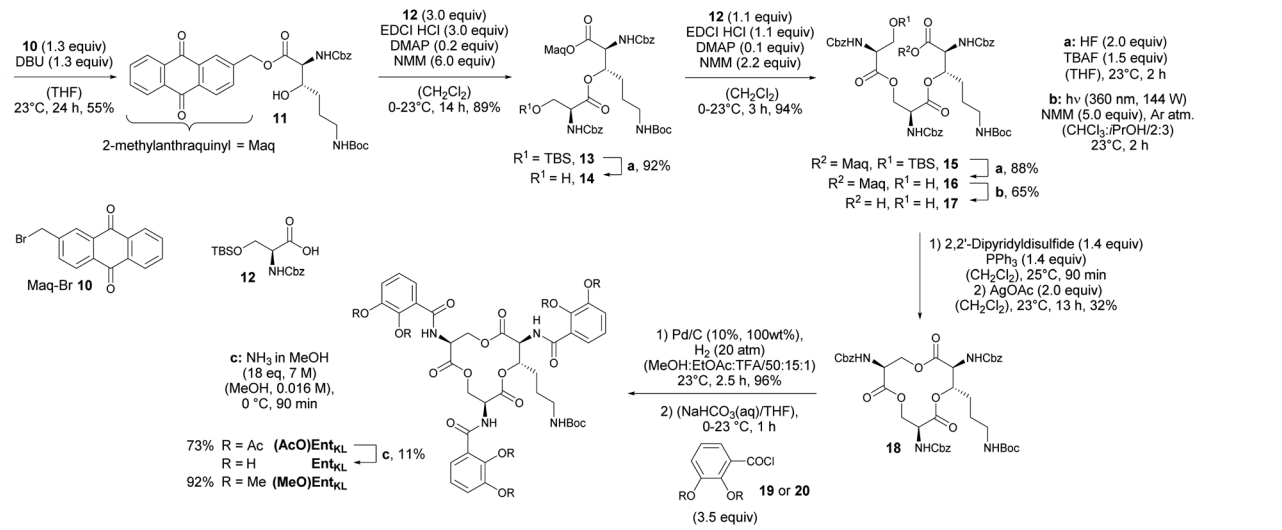

Scheme 3 Assembly of a linear trimer, cyclization and final catechol decoration.

© 2021 The Author(s). Published by the Royal Society of Chemistry

Open Access Article. Published on 17 June 2021. Downloaded on 10/3/2024 11:52:16 PM. This article is licensed under a Creative Commons Attribution-NonCommercial 3.0 Unported Licence.

Table 2 Selected conditions for the cyclization of the linear trimer **17**

Entry	Conditions	Result
1	MNBA (5.0 eq.), DMAP (8.0 eq.), (CH_2Cl_2), 0–23 °C, 20 h	13%[a]
2	PPh_3 (1.5 eq.), DIAD (1.3 eq.), (THF), 0–23 °C, 24 h	14%[a]
3	(1) Corey's disulfane[92] (1.4 eq.), PPh_3 (1.4 eq.), (CH_2Cl_2), 23 °C, 10 min; (2) $AgBF_4$ (5.0 eq.), (PhH), 25 °C, 16 h	5–50%[a,b]
4	(1) 2,2′-Dipyridyldisulfide (1.4 eq.), PPh_3 (1.4 eq.) in (CH_2Cl_2), 30 °C, 90 min; (2) AgOAc (2.0 eq.), (PhH), 30 °C, 3 h	32%[a]

[a] Elimination. [b] Bad reproducibility.

conditions. Low-micromolar concentrations of **Ent** restored growth, and the *E. coli* cultures reached $OD_{600} \approx 0.1$, 0.15 and 0.3 in the presence of 1.0 μM, 10 μM and 15 μM **Ent**, respectively (Fig. 1A).

Intriguingly, the addition of **(AcO)Ent$_{KL}$** led to restore the growth of *E. coli* K-12 Δ*entA* in the presence of DP in a concentration dependent-manner and with a similar efficiency as the natural siderophore **Ent** (Fig. 1A and B). A significant increase in growth was observed starting at 1 μM concentration, while at 10 μM and 15 μM the cultures grew to $OD_{600} \approx 0.15$ and 0.3, respectively, indicating the ability of **(AcO)Ent$_{KL}$** to be internalized into the cytosol of *E. coli*. Similarly, *P. aeruginosa* K648 Δ*pvd*/*pch* grew to $OD_{600} \approx 0.4$ (37 °C, $t = 24$ h) and this value decreased to <0.25 in the presence of 600 μM DP. Supplementation of the iron-reduced growth medium with 1.0 μM of **Ent** resulted in the restoration of *P. aeruginosa* growth to $OD_{600} \approx$ 0.35 (Fig. 1D).

At higher concentrations of **Ent** of 10 μM and 15 μM the growth promoting response was even exceeding the growth in absence of DP, with *P. aeruginosa* K648 Δ*pvd*/*pch* growing to $OD_{600} \approx 0.5$ and 0.6, respectively. Again, **(AcO)Ent$_{KL}$** was also able to restore the growth of *P. aeruginosa* K648 Δ*pvd*/*pch* under iron-limiting conditions in a concentration-dependent manner (Fig. 1D and E). While the growth promoting effect of **(AcO)Ent$_{KL}$** at a concentration of 1.0 μM was slightly smaller compared to **Ent**, the growth promoting was clearly surpassing the effect of **Ent** at 10 μM. In contrast to the uptake of **Ent** in *E. coli*, **Ent** never reaches the cytosol of *P. aeruginosa* as iron release takes place in the periplasm through cleavage of the siderophore backbone by the periplasmic esterase PfeE.[113] This indicates that the compounds are accepted as substrates by PfeE. As expected, the permethylated probe **(MeO)Ent$_{KL}$**, was not able to restore growth of neither *E. coli* K-12 Δ*entA* nor *P. aeruginosa* K648 Δ*pvd*/*pch* (Fig. 1C and F).

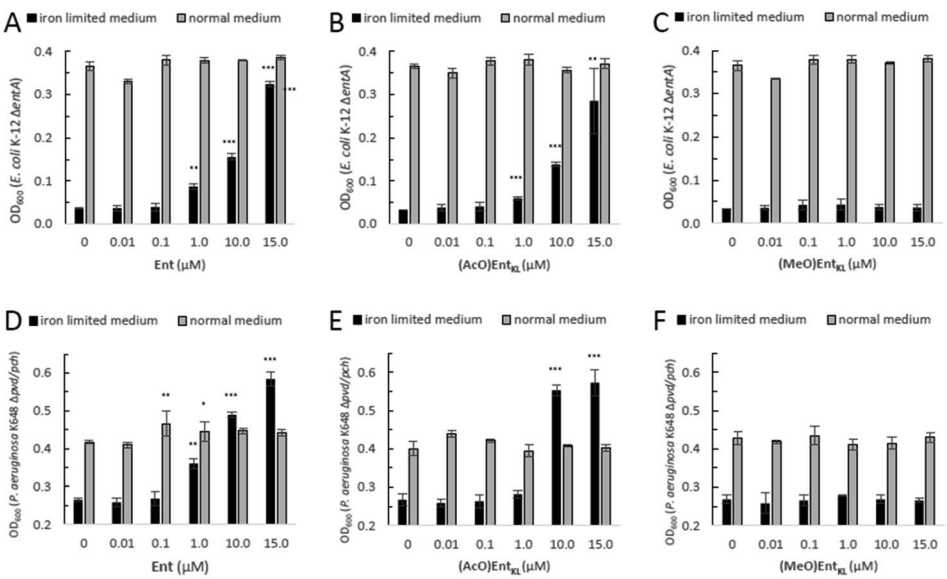

Fig. 1 *E. coli* K-12 Δ*entA* and *P. aeruginosa* K648 Δ*pvd*/*pch* growth recovery assays employing **Ent** in comparison to **(AcO)Ent$_{KL}$** and **(MeO)Ent$_{KL}$** (50% MHB II, ±200 or 600 μM DP (2,2′-bipyridine), $t = 24$ h, 37 °C). Gray bars: OD_{600} of bacteria cultured in the absence of DP. Black bars: OD_{600} of bacteria cultured in the presence of 200 μM (*E. coli*) or 600 μM (*P. aeruginosa*) DP. (A) **Ent** promotes growth recovery of *E. coli*. (B) **(AcO)Ent$_{KL}$** affords growth recovery of *E. coli*. (C) **(MeO)Ent$_{KL}$** shows no growth recovery of *E. coli*. (D) **Ent** promotes growth recovery of *P. aeruginosa*. (E) **(AcO)Ent$_{KL}$** affords growth recovery of *P. aeruginosa*. (F) **(MeO)Ent$_{KL}$** shows no growth recovery of *P. aeruginosa*. Each bar indicates the average of three independent replicates (two wells per replicate) and the error bars are the standard deviation of the mean. As *P. aeruginosa* shows a growth of <0.25 OD in the absence of an external siderophore, *Y*-axis is shown starting at an OD_{600} of 0.2. Statistical significance is indicated as a *p*-value < 0.05and was determined by an unpaired *t*-test using GraphPad Prism 9 (version 9.1.1). ***(*P*-value: <0.001), **(*P*-value: <0.005) and *(*P*-value: <0.05).

Open Access Article. Published on 17 June 2021. Downloaded on 10/3/2024 11:52:16 PM.
This article is licensed under a Creative Commons Attribution-NonCommercial 3.0 Unported Licence.

Next, we synthesized a series of cargo-conjugates of **(AcO)Ent$_{KL}$** and **(MeO)Ent$_{KL}$** attaching fluorophores and dyes that differ in their size in order to investigate whether **(AcO)Ent$_{KL}$** is able to deliver different cargo molecules to *E. coli* and *P. aeruginosa*. Therefore, we cleaved the Boc group at the amino handle in the presence of TFA in dichloromethane and reacted the resulting free amine in the presence of *N*-hydroxy succinimide (NHS) esters of the corresponding fluorophores and dyes (**SulfoCy5-NHS**, **BODIPY$_{FL}$-NHS** and **MG-NHS**) obtaining the conjugates **(AcO)Ent$_{KL}$-BODIPY$_{FL}$**, **(AcO)Ent$_{KL}$-MG** and **(AcO)Ent$_{KL}$-SulfoCy5** as well as their respective negative control probes **(MeO)Ent$_{KL}$-BODIPY$_{FL}$**, **(MeO)Ent$_{KL}$-MG** and **(MeO)Ent$_{KL}$-SulfoCy5** in moderate yields as outlined in Scheme 4. Similarly, initial Boc cleavage in the presence of TFA and subsequent installation of a PEG$_4$-N$_3$ chain *via* NHS ester coupling gave access to the corresponding **(AcO)Ent$_{KL}$-PEG$_4$-N$_3$** and **(MeO)Ent$_{KL}$-PEG$_4$-N$_3$**. Final copper(I)-mediated azide–alkyne click reaction with alkyne functionalized BODIPYs (**BODIPY-alkyne** and **BODIPY$_{FL}$-alkyne**) furnished the conjugates **(AcO)Ent$_{KL}$-PEG$_4$-BODIPY** and **(AcO)Ent$_{KL}$-PEG$_4$-BODIPY$_{FL}$** as well as their respective negative control probes **(MeO)Ent$_{KL}$-PEG$_4$-BODIPY** and **(MeO)Ent$_{KL}$-PEG$_4$-BODIPY$_{FL}$** in moderate to good yields (Scheme 4). Finally, we synthesized **(AcO)Ent$_{KL}$-PEG$_3$-MG** and **(MeO)Ent$_{KL}$-PEG$_3$-MG** *via* a sequence of initial Boc cleavage, installation of a PEG$_3$-NHBoc chain *via* NHS ester coupling, final Boc cleavage and reaction of the free amine with **MG-NHS** in moderate yields.

When incubating *E. coli* K-12 Δ*entA* under iron-limiting conditions with **(AcO)Ent$_{KL}$-PEG$_4$-BODIPY**, **(AcO)Ent$_{KL}$-PEG$_4$-BODIPY$_{FL}$**, **(AcO)Ent$_{KL}$-BODIPY$_{FL}$** and **(AcO)Ent$_{KL}$-SulfoCy5** led to a concentration-dependent growth recovery (Fig. 2A–D) clearly indicating the uptake of these cargo-conjugates to the cytosol of *E. coli*. The two conjugates **(AcO)Ent$_{KL}$-MG** and **(AcO)Ent$_{KL}$-PEG$_3$-MG** bearing a malachite green derivative as cargo molecule did not lead to a growth recovery in *E. coli* (Fig. 2E and F). Furthermore, high concentrations of 10 μM and 15 μM seemed to reduce overall growth in *E. coli* K-12 Δ*entA* (Fig. 1E and F) as well as in the *E. coli* wild-type strain (see ESI: Fig. S7

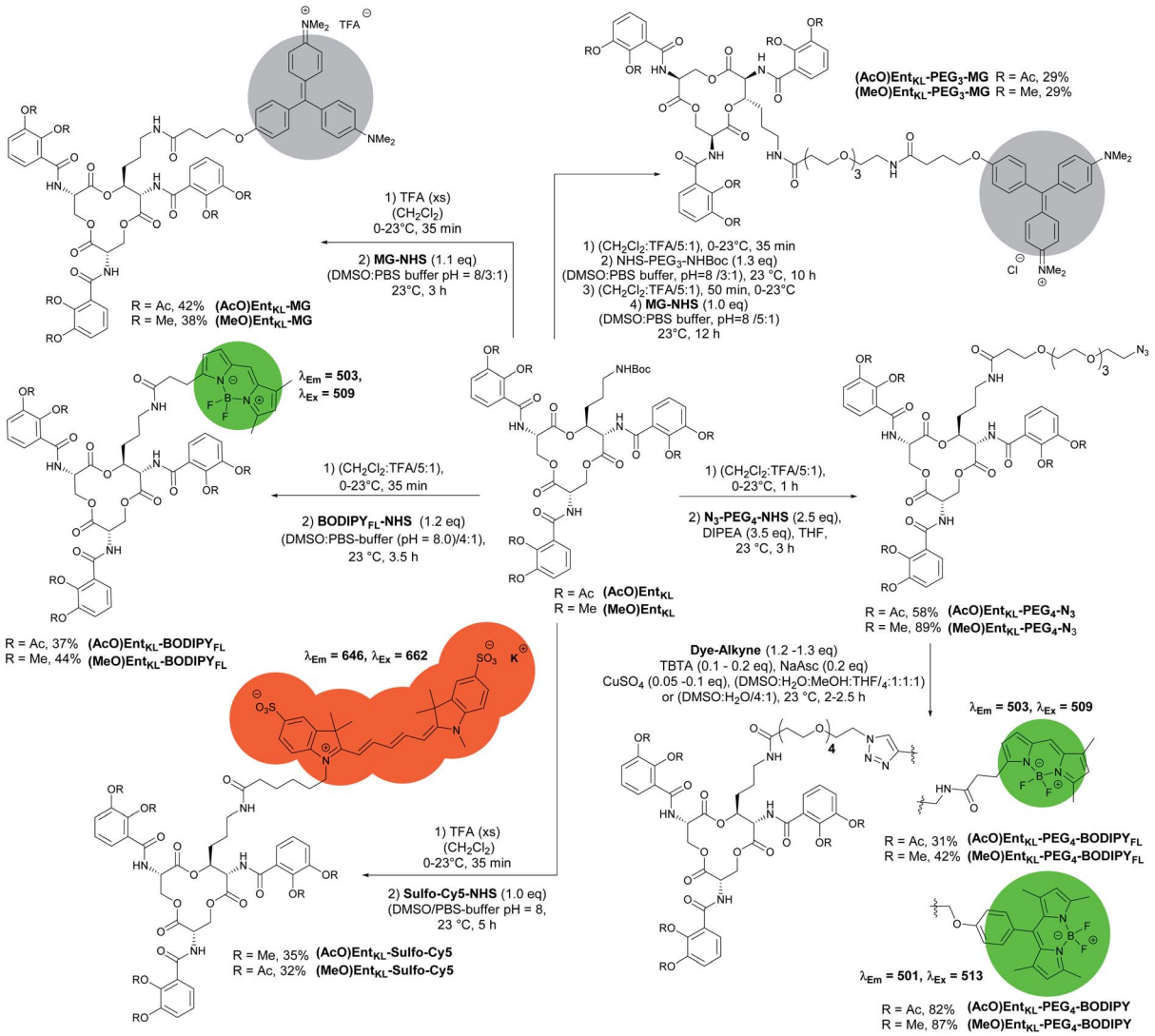

Scheme 4 Synthesis of different Ent$_{KL}$-cargo conjugates bearing different fluorophores and chromophores as payload.

© 2021 The Author(s). Published by the Royal Society of Chemistry

Open Access Article. Published on 17 June 2021. Downloaded on 10/3/2024 11:52:16 PM.
This article is licensed under a Creative Commons Attribution-NonCommercial 3.0 Unported Licence.

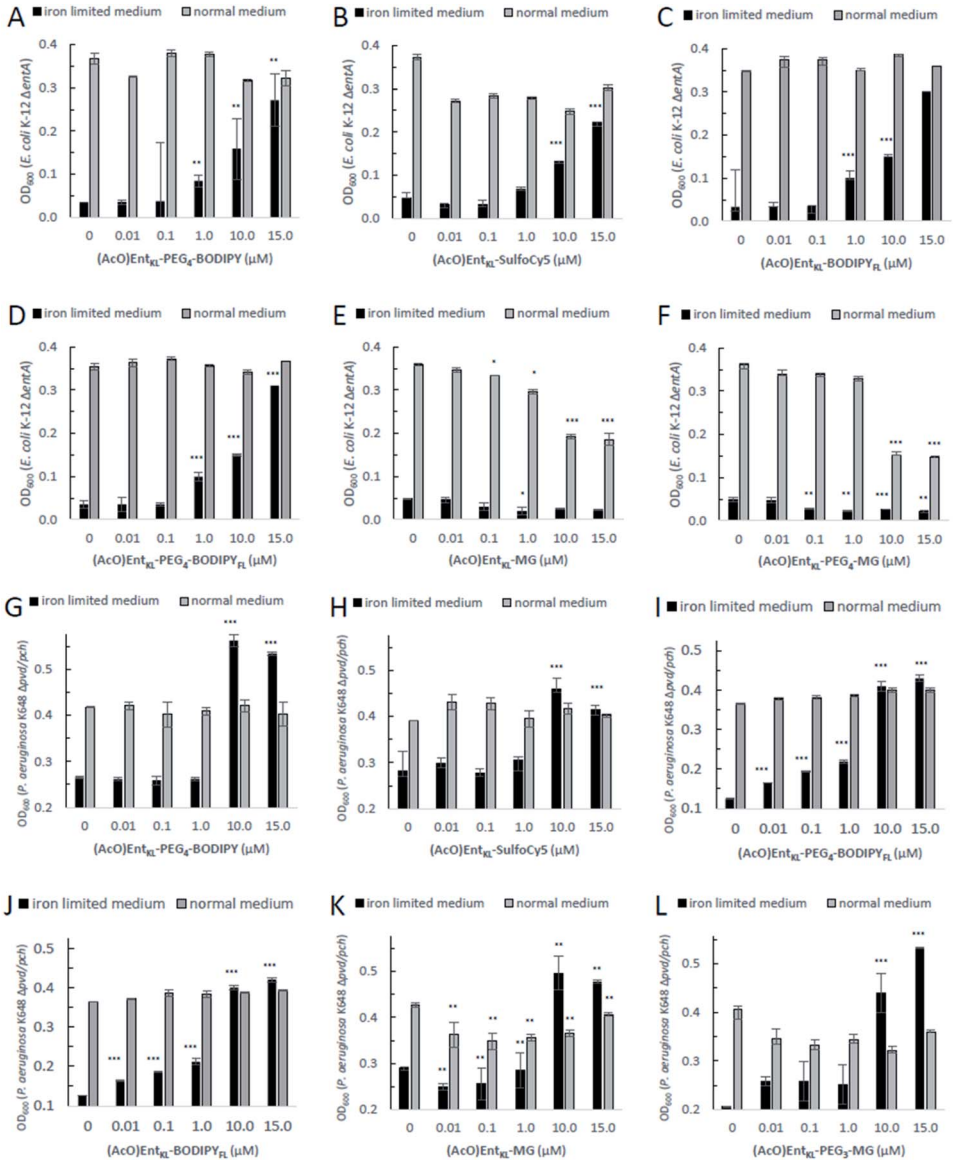

Fig. 2 *E. coli* K-12 Δ*entA* (A–F) and *P. aeruginosa* K648 Δ*pvd*/*pch* (G–L) growth recovery assays employing **(AcO)Ent$_{KL}$-PEG$_4$-BODIPY**, **(AcO)Ent$_{KL}$-BODIPY$_{FL}$**, **(AcO)Ent$_{KL}$-PEG$_4$-BODIPY$_{FL}$**, **(AcO)Ent$_{KL}$-SulfoCy5**, **(AcO)Ent$_{KL}$-MG** and **(AcO)Ent$_{KL}$-PEG$_3$-MG** (50% MHB II, ± 200 or 600 μM DP (2,2′-bipyridine), t = 24 h, 30 °C). Gray bars: OD_{600} of bacteria cultured in the absence of DP. Black bars: OD_{600} of bacteria cultured in the presence of 200 μM (*E. coli*) or 600 μM (*P. aeruginosa*) DP. (A) **(AcO)Ent$_{KL}$-PEG$_4$-BODIPY** promotes growth recovery of *E. coli*. (B) **(AcO)Ent$_{KL}$-SulfoCy5** promotes growth recovery of *E. coli*. (C) **(AcO)Ent$_{KL}$-BODIPY$_{FL}$** promotes growth recovery of *E. coli*. (D) **(AcO)Ent$_{KL}$-PEG$_4$-BODIPY$_{FL}$** promotes growth recovery of *E. coli*. (E) **(AcO)Ent$_{KL}$-MG** is not able to restore growth of *E. coli*. (F) **(AcO)Ent$_{KL}$-PEG$_3$-MG** is not able to restore growth of *E. coli*. As *P. aeruginosa* shows a growth of <0.25 OD in the absence of an external siderophore, *Y*-axis is shown starting at an OD_{600} of 0.2. (G) **(AcO)Ent$_{KL}$-PEG$_4$-BODIPY** promotes growth recovery of *P. aeruginosa*. (H) **(AcO)Ent$_{KL}$-SulfoCy5** promotes growth recovery of *P. aeruginosa*. (I) **(AcO)Ent$_{KL}$-BODIPY$_{FL}$** promotes growth recovery of *P. aeruginosa*. (J) **(AcO)Ent$_{KL}$-PEG$_4$-BODIPY$_{FL}$** promotes growth recovery of *P. aeruginosa*. (K) **(AcO)Ent$_{KL}$-MG** promotes growth recovery of *P. aeruginosa*. (L) **(AcO)Ent$_{KL}$-PEG$_3$-MG** promotes growth recovery of *P. aeruginosa*. Each bar indicates the average of three independent replicates (two wells per replicate) and the error bars are the standard deviation of the mean. Fig. S3–S8 (see ESI)† contain the assay results for the corresponding negative control probes **(MeO)EntKL-PEG4-BODIPY**, **(MeO)Ent$_{KL}$-BODIPYFL**, **(MeO)Ent$_{KL}$-PEG$_4$-BODIPYFL**, **(MeO)Ent$_{KL}$-SulfoCy5**, **(MeO)Ent$_{KL}$-MG** and **(MeO)Ent$_{KL}$-PEG$_3$-MG**, none of which were able to restore growth in neither *E. coli* nor *P. aeruginosa*. Statistical significance is indicated as a p-value < 0.05 and was determined by an unpaired t-test using GraphPad Prism 9 (version 9.1.1). ***(P-value: <0.001), **(P-value: <0.005) and *(P-value: <0.05).

and S8†). This might be due to the fact that these compounds are not taken up by the bacteria and therefore, they further reduce the available iron in the surrounding medium. Although, the malachite green derivative attached within **(AcO)Ent$_{KL}$-MG** and **(AcO)Ent$_{KL}$-PEG$_3$-MG** has a large diameter of approximately 13.7 Å (extracted from an energy minimized structure by Chem3D® Ultra 15.1.0.144), size seems not to be the exclusive parameter for uptake. In comparison, **(AcO)Ent$_{KL}$-SulfoCy5**, bearing the rigid **SulfoCy5** fluorophore with a length diameter of approximately 19.9 Å (extracted from an energy

Open Access Article. Published on 17 June 2021. Downloaded on 10/3/2024 11:52:16 PM.
This article is licensed under a Creative Commons Attribution-NonCommercial 3.0 Unported Licence.

minimized structure by Chem3D® Ultra 15.1.0.144) of its indocyanine-backbone, led to a growth recovery under same conditions. Looking at the crystal structure of the enterobactin specific siderophore receptor FepA,[79] the transmembrane pore opening upon recognition of **Ent** seems to have an elliptical inner diameter between 20-30 Å, large enough to harbor any of the reported conjugated discussed here. Therefore, additional parameters beyond size seem to determine the uptake of a bound cargo at the outer membrane receptor.

However, size exclusion might still play a role at the ABC-type transporter mediating uptake of hydrolyzed fragments across the inner membrane.

When incubating the conjugates with *P. aeruginosa* K648 Δ*pvd*/*pch* under iron-limiting media conditions all cargo conjugates led to clear concentration-dependent growth recovery, including **(AcO)Ent$_{KL}$-MG** and **(AcO)Ent$_{KL}$-PEG$_3$-MG**, indicating the uptake of these cargo-conjugates to the periplasm of *P. aeruginosa* (Fig. 2G–L). These results are in line with the findings of Nolan and co-workers[42] reporting that *P. aeruginosa* exhibits greater promiscuity for the uptake compared to *E. coli*. Looking at the crystal structure of PfeA,[69] the outer membrane siderophore receptor of *P. aeruginosa*, a similar elliptical inner diameter between 25–35 Å can be assumed. Consistently, none of the corresponding permethylated negative control probes led to a growth recovery neither in *E. coli* nor *P. aeruginosa* (see ESI, Fig. S3–S8†). The overall growth recovery response to the added compounds was significantly higher for *P. aeruginosa* K648 Δ*pvd*/*pch* compared to *E. coli* K-12 Δ*entA*, under non-iron-limiting conditions (Fig. 3B). The comparison of the growth recovery over all tested compounds in *E. coli* revealed a similar effciency of all conjugates compared to the natural siderophore **Ent** (Fig. 3A).

A similar picture was observed for the growth recovery in *P. aeruginosa*. However, for some of the compounds such as **(AcO)Ent$_{KL}$** and **(AcO)Ent$_{KL}$-PEG$_4$-BODIPY** an even improved performance compared to **Ent** was observed (Fig. 3B). Furthermore, we were able to demonstrate that growth of *P. aeruginosa* mutants could be restored with **(AcO)Ent$_{KL}$** in the presence of comparably high concentrations (0.01 μM, 0.1 μM, 1.0 μM and 10 μM) of the human iron scavenger protein apo-transferrin ($K_d = 10^{-22}$ M)[114] (see ESI, Fig. S9†).

Further, an additional growth recovery assay was conducted with **(AcO)Ent$_{KL}$** in the presence of high concentrations (1.0 μM, 10.0 μM, 50 μM and 100 μM) bovine serum albumin (see ESI, Fig. S9†). It is worth to mention, that growth recovery was achieved with **(AcO)Ent$_{KL}$**. Albumin is responsible for the transport of lipophilic compounds and it is therefore able to bind **Ent**[115] These results indicate the potential ability of our designed enterobactin derivative **(AcO)Ent$_{KL}$** to compete with human iron-binding and lipophilic transport serum proteins.

Next, we incubated **(AcO)Ent$_{KL}$-BODIPY$_{FL}$**, **(MeO)Ent$_{KL}$-BODIPY$_{FL}$**, **(AcO)Ent$_{KL}$-PEG$_4$-BODIPY$_{FL}$** and **(MeO)Ent$_{KL}$-PEG$_4$-BODIPY$_{FL}$** at different concentrations with *E. coli* K-12 Δ*entA*, *P. aeruginosa* K648 Δ*pvd*/*pch* and their corresponding wild-type strains under iron-limiting conditions in order to proof whether uptake of the probes leads to fluorescence labelling of the bacteria, providing additional evidence for the uptake into the bacteria.[115]

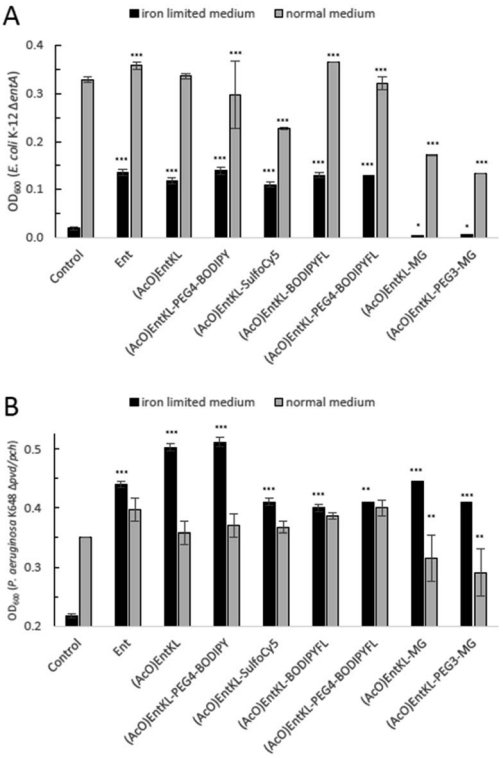

Fig. 3 Comparison of *E. coli* K-12 Δ*entA* (A) and *P. aeruginosa* K648 Δ*pvd*/*pch* (B) growth recovery assays employing 10 μM concentration of (AcO)Ent$_{KL}$-PEG$_4$-BODIPY, (AcO)Ent$_{KL}$-BODIPY$_{FL}$, (AcO)Ent$_{KL}$-PEG$_4$-BODIPY$_{FL}$, (AcO)Ent$_{KL}$-SulfoCy5, (AcO)Ent$_{KL}$-MG and (AcO)Ent$_{KL}$-PEG$_3$-MG under iron-limiting and non-limiting conditions (50% MHB II, ±200 or 600 μM DP (2,2′-bipyridine), t = 24 h, 37 °C). Gray bars: OD_{600} of bacteria cultured in the absence of DP. Black bars: OD_{600} of bacteria cultured in the presence of 200 μM (*E. coli*) or 600 μM (*P. aeruginosa*) DP. Each bar indicates the average of three independent replicates (two wells per replicate) and the error bars are the standard deviation of the mean. As *P. aeruginosa* shows a growth of <0.25 OD in the absence of an external siderophore, *Y*-axis is shown starting at an OD_{600} of 0.2. Statistical significance is indicated as a *p*-value < 0.05and was determined by an unpaired *t*-test using GraphPad Prism 9 (version 9.1.1). ***(*P*-value: <0.001), **(*P*-value: <0.005) and *(*P*-value: <0.05).

To our delight, all assessed bacteria were fluorescently labelled when treated with either **(AcO)Ent$_{KL}$-PEG$_4$-BODIPY$_{FL}$** or **(AcO)Ent$_{KL}$-BODIPY$_{FL}$** at concentrations of 10 μM (Fig. 4A, B, D and E, see ESI, Fig. S11, S13, S16 and S18†), further confirming the uptake into the wild-type and mutant strains of *E. coli* and *P. aeruginosa*. Weaker fluorescence was observed at 1.0 μM concentration of the fluorophore conjugates on all tested strains (see ESI, Fig. S11, S13, S16, S18 and Table S3†). In general, the fluorescence uptake into both mutant strains was higher compared to the wild types, and *E. coli* showed a significantly higher uptake than *P. aeruginosa* (see ESI, Table S3†).

Furthermore, we observed slight differences in the labeling performance of **(AcO)Ent$_{KL}$-BODIPY$_{FL}$** and **(AcO)Ent$_{KL}$-PEG$_4$-BODIPY$_{FL}$** for the different bacteria. While **(AcO)Ent$_{KL}$-BODIPY$_{FL}$** led to more prominent labelling of *E. coli* BW25113

© 2021 The Author(s). Published by the Royal Society of Chemistry

Open Access Article. Published on 17 June 2021. Downloaded on 10/3/2024 11:52:16 PM.
This article is licensed under a Creative Commons Attribution-NonCommercial 3.0 Unported Licence.

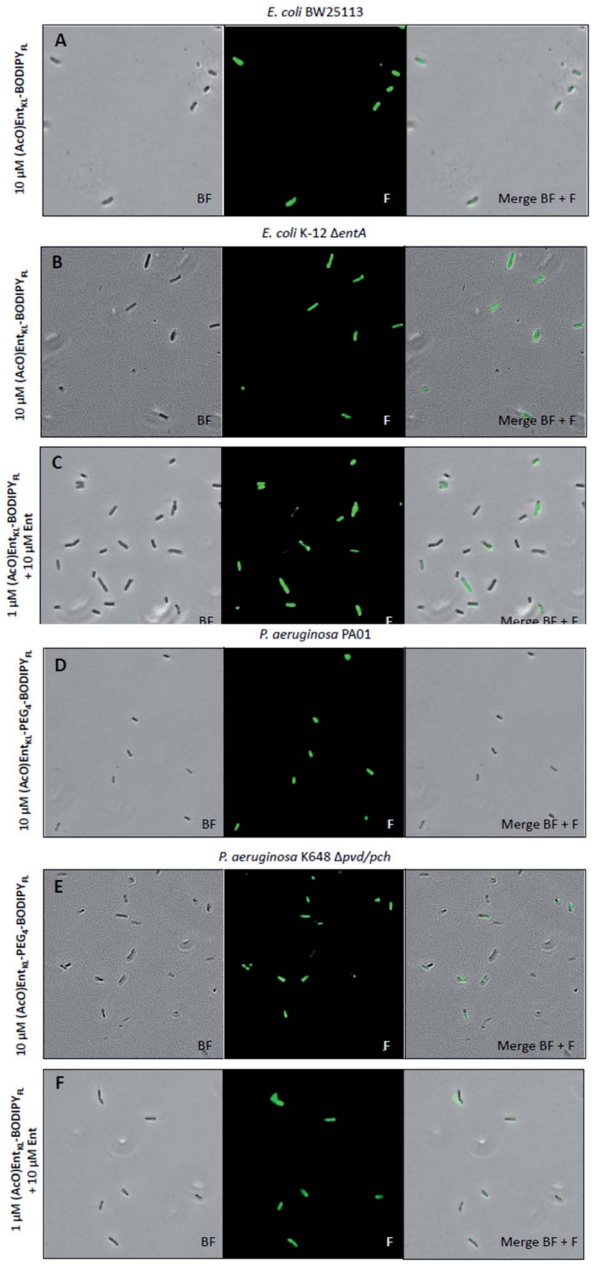

Fig. 4 Fluorescence microscopy of *E. coli* BW25113, *E. coli* K-12 Δ*entA*, *P. aeruginosa* PA01 and *P. aeruginosa* K468 Δ*pch/pvd* cultivated under iron-limiting conditions (50% MHB II, +200 or 600 μM DP (2,2′-bipyridine), $t = 24$ h, 37 °C) and treated with 10 μM of **(AcO)Ent$_{KL}$-BODIPY$_{FL}$** (A and B), 10 μM of **(AcO)Ent$_{KL}$-PEG$_4$-BODIPY$_{FL}$** (D and E) or a mixture **(AcO)Ent$_{KL}$-BODIPY$_{FL}$** (1 μM) : **Ent** (10 μM) (C and F). All images were captured using a 40×/1.30 objective (overall magnification of 400×). BF: bright field, F: fluorescence GFP filter set (excitation: 480 nm, 20 nm bandwidth; emission: 527 nm, 15 nm bandwidth). For corrected total cell fluorescence (CTCF) of each experiment see Table S3 in the ESI.†

and *E. coli* K-12 Δ*entA*, **(AcO)Ent$_{KL}$-PEG$_4$-BODIPY$_{FL}$** preferred of *P. aeruginosa* PA01 and *P. aeruginosa* K468 Δ*pvd/pch* (see ESI, Table S3†). Consistently, no labelling was observed when cells were treated with either **(MeO)Ent$_{KL}$-BODIPY$_{FL}$**, **(MeO)Ent$_{KL}$-PEG$_4$-BODIPY$_{FL}$** or non-conjugated **BODIPY$_{FL}$-alkyne** alone (see ESI, Fig. S12, S14, S15, S17, S19 and S20†). Fluorescence labeling of *E. coli* K-12 Δ*entA* and *P. aeruginosa* K468 Δ*pvd/pch* was also observed when treating the bacteria with mixtures of **(AcO)Ent$_{KL}$-BODIPY$_{FL}$** : **Ent**/1 : 10, 1 : 1, 10 : 1 or 10 : 10 (Fig. S21 and S22†).

Interestingly, the fluorescence labelling for *E. coli* and *P. aeruginosa* mutant strains seems to be increased in the presence of **Ent**, as lower concentrations of 1.0 μM of the fluorophore conjugates led to strong fluorescence signals of similar intensity (Fig. 4C and F, see also ESI, Table S3†) compared to the 10-fold higher concentration in absence of **Ent** (Fig. 4B and E, see also ESI, Table S3†). We assume that the overall fitness of the bacteria is increased in the presence of additional siderophore, leading to a more efficient uptake of the fluorophore conjugates. These results underline the potential of **Ent$_{KL}$**-based reporter conjugates to serve as molecular tools for infection detection.

Finally, **(AcO)Ent$_{KL}$**, **(MeO)Ent$_{KL}$** and all derived cargo-conjugates were investigated for their antibacterial activity against the *E. coli* and *P. aeruginosa* strains and the compounds' cytotoxic activity against human HepG2 cells was assessed (see ESI, Table S4†). All tested compounds lack antibacterial and cytotoxic activity, which is important looking at **(AcO)Ent$_{KL}$** in the context of being potentially used as safe carrier molecule for the future development of antimicrobial siderophore drug conjugates that help to prevent fast resistance development. In addition, all compounds lack any cytotoxic activity against human HepG2 cells, enabling their possible application in mammalian cells. Notably, although the close derivative of Miller's artificial enterobactin analogue[47] **(AcO)Ent$_{M}$** displayed similar growth recovery efficacy in siderophore biosynthesis deficient mutants of *E. coli* and *P. aeruginosa* compared to **(AcO)Ent$_{KL}$** (see ESI, Fig. S10†), we found significant cytotoxic activity against human HepG2 cells with an IC_{50} value of 12.17 μM in our assay (see ESI, Table S4†).

Conclusions

In summary, we designed and synthesized the novel enterobactin derivative **(AcO)Ent$_{KL}$**, which retains the natural hydrolyzability of the tris-lactone scaffold, while providing an amino handle for easy attachment of cargos in the backbone. *In silico* studies at the DFT level of theory predicted a high thermodynamic stability combined with kinetic lability for the iron(III) complexes similarly as demonstrated earlier for the natural ferri-siderophore **[Fe-Ent]$^{3-}$**.

Growth recovery experiments with siderophore biosynthesis deficient mutants of *E. coli* and *P. aeruginosa* under iron-limiting conditions revealed an uptake of **(AcO)Ent$_{KL}$** and other **Ent$_{KL}$**-based derivatives into the tested bacteria, while, in contrast, permethylated probes based on **(MeO)Ent$_{KL}$** unable to bind iron, did not lead to any growth recovery.

Furthermore, imaging experiments under iron-limiting conditions utilizing *E. coli* and *P. aeruginosa* deficient mutants and wild-type strains showed labelling of the bacteria, further underlining the uptake of cargo conjugates.

© 2021 The Author(s). Published by the Royal Society of Chemistry

Open Access Article. Published on 17 June 2021. Downloaded on 10/3/2024 11:52:16 PM. This article is licensed under a Creative Commons Attribution-NonCommercial 3.0 Unported Licence.

As fluorophore uptake into both, *E. coli* K-12 Δ*entA* and *P. aeruginosa* K648 Δ*pvd*/*pch*, was increased in the presence of supplemented **Ent**, we assume that overexpression of **Ent** would not contribute to any resistance against $\mathbf{Ent_{KL}}$-based drug conjugates.

Since growth recovery was also observed in the presence of high concentrations of human apo-transferrin or albumin and no antimicrobial activity or cytotoxicity was observed, **(AcO)** $\mathbf{Ent_{KL}}$ holds potential to serve as good starting point for the assembly of antimicrobial siderophore drug conjugates to tackle infections caused by Gram-negative bacterial pathogens in humans.

Further investigations towards the determination of the size exclusion limit of siderophore receptors and the synthesis of first drug conjugates are ongoing.

Data availability

All data are available in the ESI.

Author contributions

The research was conceived by P. K. The manuscript was written by P. K. with contributions of R. Z., J. C., J. G. and R. M. The ESI† was written by R. Z., P. K., J. C., J. H., J. G. and R. M. All compounds were synthesized by R. Z. Computations were planned by J. G. and conducted by J. V. Biological evaluation of the compounds was planned by J. H., R. M., J. C. and P. K. and conducted by J. C. All authors have given approval to the final version of the manuscript.

Conflicts of interest

There are no conflicts to declare.

Acknowledgements

This work has been carried out within the framework of the SMART BIOTECS alliance between the Technische Universität Braunschweig and the Leibniz Universität Hannover. This initiative is supported by the Ministry of Science and Culture (MWK) of Lower Saxony, Germany. Financially support by the DFG (Grant KL3012/2-1) and Fonds der Chemischen Industrie is gratefully acknowledged. The content of this work is solely the responsibility of the authors and does not necessarily represent the official views of the funding agencies. The authors thank Prof. Dr Mark Brönstrup from the Helmholtz Centre of Infection Research for kindly providing bacterial strains used in this study. The authors thank the mass spectrometry unit of the Institute of Organic Chemistry at the TU Braunschweig, in particular Dr Ulrich Papke, the NMR spectroscopy unit of the Institute of Organic Chemistry, in particular Dr Kerstin Ibrom, for analytical support, Alexandra Amann for support in the biological evaluation of the compounds as well as Claire C. Jimidar, Charity S. G. Ganskow, Dr Elmira Ghabraie, Prof. Dr Stefan Schulz and Dr Anna Luisa Klahn for helpful discussion and proofreading of the manuscript.

Notes and references

1 P. Klahn and M. Brönstrup, *Curr. Top. Microbiol. Immunol.*, 2016, **389**, 365–417.
2 V. M. D'Costa, C. E. King, L. Kalan, M. Morar, W. W. L. Sung, C. Schwarz, D. Froese, G. Zazula, F. Calmels, R. Debruyne, G. B. Golding, H. N. Poinar and G. D. Wright, *Nature*, 2011, **477**, 457–461.
3 K. M. G. O'Connell, J. T. Hodgkinson, H. F. Sore, M. Welch, G. P. C. Salmond and D. R. Spring, *Angew. Chem., Int. Ed.*, 2013, **52**, 10706–10733.
4 P. Klahn and M. Brönstrup, *Nat. Prod. Rep.*, 2017, **34**, 832–885.
5 U. Theuretzbacher, K. Outterson, A. Engel and A. Karlen, *Nat. Rev. Microbiol.*, 2020, **18**, 275–285.
6 H. W. Boucher, G. H. Talbot, D. K. Benjamin, J. Bradley, R. J. Guidos, R. N. Jones, B. E. Murray, R. A. Bonomo and D. Gilbert, *Clin. Infect. Dis.*, 2013, **56**, 1685–1694.
7 H. W. Boucher, G. H. Talbot, J. S. Bradley, J. E. Edwards, D. Gilbert, L. B. Rice, M. Scheld, B. Spellberg and J. Bartlett, *Clin. Infect. Dis.*, 2009, **48**, 1–12.
8 WHO, *Prioritization of pathogens to guide discovery, research and development of new antibiotics for drug-resistant bacterial infections, including tuberculosis*, World Health Organization, Geneva, WHO/EMP/IAU/2017.12, 2017.
9 G. Zhou, Q. Shi, X. Huang and X. Xie, *Int. J. Mol. Sci.*, 2015, **16**, 21711–21733.
10 Y.-M. Lin, M. Ghosh, P. A. Miller, U. Möllmann and M. J. Miller, *BioMetals*, 2019, **32**, 425–451.
11 A. V. Cheng and W. M. Wuest, *ACS Infect. Dis.*, 2019, **5**, 816–828.
12 M. J. Miller and R. Liu, *Acc. Chem. Res.*, 2021, **54**, 1646–1661.
13 R. C. Hider and X. Kong, *Nat. Prod. Rep.*, 2010, **27**, 637–657.
14 K. N. Raymond, E. A. Dertz and S. S. Kim, *Proc. Natl. Acad. Sci. U. S. A.*, 2003, **100**, 3584–3588.
15 M. Sánchez, L. Sabio, N. Gálvez, M. Capdevila and J. M. Dominguez-Vera, *IUBMB Life*, 2017, **69**, 382–388.
16 T. C. Johnstone and E. M. Nolan, *Dalton Trans.*, 2015, **44**, 6320–6339.
17 V. I. Holden and M. A. Bachman, *Metallomics*, 2015, **7**, 986–995.
18 P. Saha, B. S. Yeoh, R. A. Olvera, X. Xiao, V. Singh, D. Awasthi, B. C. Subramanian, Q. Chen, M. Dikshit, Y. Wang, C. A. Parent and M. Vijay-Kumar, *J. Immunol.*, 2017, **198**, 4293–4303.
19 J. Behnsen and M. Rafatellu, *MBio*, 2016, **7**, e01906-16.
20 V. Braun and M. Braun, *FEBS Lett.*, 2002, **529**, 78–85.
21 P. E. Klebba, *Front. Biosci.*, 2003, **8**, 1422–1436.
22 L. Ma, W. Kaserer, R. Annamalai, D. C. Scott, B. Jin, X. Jiang, Q. Xiao, H. Maymani, L. M. Massis, L. C. S. Ferreira, S. M. C. Newton and P. E. Klebba, *J. Biol. Chem.*, 2007, **282**, 397–406.
23 C. R. Smallwood, L. Jordan, V. Trinh, D. W. Schuerch, A. Gala, M. Hanson, Y. Shipelskiy, A. Majumdar, S. M. C. Newton and P. E. Klebba, *J. Gen. Physiol.*, 2014, **144**, 71–80.

© 2021 The Author(s). Published by the Royal Society of Chemistry

Open Access Article. Published on 17 June 2021. Downloaded on 10/3/2024 11:52:16 PM. This article is licensed under a Creative Commons Attribution-NonCommercial 3.0 Unported Licence.

24 A. S. Skwarecki, S. Milewski, M. Schielmann and M. J. Milewska, *Nanomedicine*, 2016, **12**, 2215–2240.
25 C. Ji, R. E. Juárez-Hernández and M. J. Miller, *Future Med. Chem.*, 2012, **4**, 297–313.
26 M. G. P. Page, *Ann. N. Y. Acad. Sci.*, 2013, **1277**, 115–126.
27 K. Li, W. H. Chen and S. D. Bruner, *BioMetals*, 2016, **29**, 377–388.
28 K. H. Negash, J. K. S. Norris and J. T. Hodgkinson, *Molecules*, 2019, **24**, 3314.
29 I. J. Schalk, *Clin. Microbiol. Infect.*, 2018, **24**, 801–802.
30 V. Braun, A. Pramanik, T. Gwinner, M. Köberle and E. Bohn, *BioMetals*, 2009, **22**, 3–13.
31 H. Budzikiewicz, *Curr. Top. Med. Chem.*, 2001, **1**, 73–82.
32 A. Górska, A. Sloderbach and M. P. Marszałł, *Trends Pharmacol. Sci.*, 2014, **35**, 442–449.
33 T. A. Wencewicz and M. J. Miller, in *Antibacterials. Topics in Medicinal Chemistry*, ed. J. Fisher, S. Mobashery and M. J. Miller, Springer, Cham, 2017, vol. 26.
34 V. Braun, K. Gunthner, K. Hantke and L. Zimmermann, *J. Bacteriol.*, 1983, **156**, 308–315.
35 A. Hartmann, H.-P. Fiedler and V. Braun, *Eur. J. Biochem.*, 1979, **99**, 517–524.
36 A. Pramanik and V. Braun, *J. Bacteriol.*, 2006, **188**, 3878–3886.
37 E. M. Nolan and C. T. Walsh, *Biochemistry*, 2008, **47**, 9289–9299.
38 S. Duquesne, D. Destoumieux-Garzón, J. Peduzzi and S. Rebuffat, *Nat. Prod. Rep.*, 2007, **24**, 708–734.
39 D. Destoumieux-Garzón, J. Peduzzi, X. Thomas, C. Djediat and S. Rebuffat, *BioMetals*, 2006, **19**, 181–191.
40 X. Thomas, D. Destoumieux-Garzón, J. Peduzzi, C. Afonso, A. Blond, N. Birlirakis, C. Goulard, L. Dubost, R. Thai, J. C. Tabet and S. Rebuffat, *J. Biol. Chem.*, 2004, **279**, 28233–28242.
41 J. D. Palmer, B. M. Mortzfeld, E. Piattelli, M. W. Silby, B. A. McCormick and V. Bucci, *ACS Infect. Dis.*, 2020, **6**, 672–679.
42 T. Zheng, J. L. Bullock and E. M. Nolan, *J. Am. Chem. Soc.*, 2012, **134**, 18388–18400.
43 T. Zheng and E. M. Nolan, *J. Am. Chem. Soc.*, 2014, **136**, 9677–9691.
44 T. A. Wencewicz, U. Möllmann, T. E. Long and M. J. Miller, *BioMetals*, 2009, **22**, 633–648.
45 M. J. Miller, A. J. Walz, H. Zhu, C. Wu, G. Moraski, U. Möllmann, E. M. Tristani, A. L. Crumbliss, M. T. Ferdig, L. Checkley, R. L. Edwards and H. I. Boshoff, *J. Am. Chem. Soc.*, 2011, **133**, 2076–2079.
46 W. Neumann and E. M. Nolan, *J. Biol. Inorg Chem.*, 2018, **23**, 1025–1036.
47 H. Kong, W. Cheng, H. Wei, Y. Yuan, Z. Yang and X. Zhang, *Eur. J. Med. Chem.*, 2019, **182**, 111615.
48 C. Ji, P. A. Miller and M. J. Miller, *J. Am. Chem. Soc.*, 2012, **134**, 9898–9901.
49 P. Chairatana, T. Zheng and E. M. Nolan, *Chem. Sci.*, 2015, **6**, 4458–4471.
50 M. Ghosh, Y.-M. Lin, P. A. Miller, U. Möllmann, W. Boggess and M. J. Miller, *ACS Infect. Dis.*, 2018, **4**, 1529–1535.
51 M. Ghosh, P. A. Miller, U. Möllmann, W. D. Claypool, V. A. Schroeder, W. R. Wolter, M. Suckow, H. Yu, S. Li, W. Huang, J. Zajicek and M. J. Miller, *J. Med. Chem.*, 2017, **60**, 4577–4583.
52 W. Neumann, M. Sassone-Corsi, M. Raffatellu and E. M. Nolan, *J. Am. Chem. Soc.*, 2018, **140**, 5193–5201.
53 W. Neumann and E. M. Nolan, *J. Biol. Inorg Chem.*, 2018, **23**, 1025–1036.
54 T. A. Wencewicz, T. E. Long, U. Möllmann and M. J. Miller, *Bioconjugate Chem.*, 2013, **24**, 473–486.
55 S. Wittmann, M. Schnabelrauch, I. Scherlitz-Hofmann, U. Möllmann, D. Ankel-Fuchs and L. Heinisch, *Bioorg. Med. Chem.*, 2002, **10**, 1659–1670.
56 M. Ghosh, P. A. Miller and M. J. Miller, *J. Antibiot.*, 2019, **73**, 152–157.
57 R. Liu, P. A. Miller, S. B. Vakulenko, N. K. Stewart, W. C. Boggess and M. J. Miller, *J. Med. Chem.*, 2018, **61**, 3845–3854.
58 M. G. P. Page, *Clin. Infect. Dis.*, 2019, **69**, S529–S537.
59 R. C. Scarrow, D. J. Ecker, C. Ng, S. Liu and K. N. Raymond, *Inorg. Chem.*, 1991, **30**, 900–906.
60 L. D. Loomis and K. N. Raymond, *Inorg. Chem.*, 1991, **30**, 906–911.
61 S. I. Müller, M. Valdebenito and K. Hantke, *BioMetals*, 2009, **22**, 691–695.
62 M. A. Fischbach, H. Lin, D. R. Liu and C. T. Walsh, *Nat. Chem. Biol.*, 2006, **2**, 132–138.
63 C. Guo, L. K. Steinberg, M. Cheng, J. H. Song, J. P. Henderson and M. L. Gross, *ACS Chem. Biol.*, 2020, **15**, 1154–1160.
64 S. M. Payne and I. B. Neilands, *Crit. Rev. Microbiol.*, 1988, **16**, 81–111.
65 H. P. Fiedler, P. Krastel, J. Müller, K. Gebhardt and A. Zeeck, *FEMS Microbiol. Lett.*, 2001, **196**, 147–151.
66 B. Ghysels, U. Ochsner, U. Möllman, L. Heinisch, M. Vasil, P. Cornelis and S. Matthijs, *FEMS Microbiol. Lett.*, 2005, **246**, 167–174.
67 K. Poole, L. Young and S. Neshat, *J. Bacteriol.*, 1990, **172**, 6991–6996.
68 C. R. Dean, S. Neshat and K. Poole, *J. Bacteriol.*, 1996, **178**, 5361–5369.
69 L. Moynié, S. Milenkovic, G. L. A. Mislin, V. Gasser, G. Malloci, E. Baco, R. P. Mccaughan, M. G. P. Page, I. J. Schalk, M. Ceccarelli and J. H. Naismith, *Nat. Commun.*, 2019, **10**, 3673.
70 W. Zhu, M. G. Winter, L. Spiga, D. P. Beiting, L. V Hooper, S. E. Winter, W. Zhu, M. G. Winter, L. Spiga, E. R. Hughes, R. Chanin, A. Mulgaonkar, L. V Hooper and S. E. Winter, *Cell Host Microbe*, 2020, **27**, 1–13.
71 M. Petrik, C. Zhai, H. Haas and C. Decristoforo, *Clin. Transl. Imaging*, 2017, **5**, 15–27.
72 R. Nosrati, S. Dehghani, B. Karimi, M. Yousefi, S. M. Taghdisi, K. Abnous, M. Alibolandi and M. Ramezani, *Biosens. Bioelectron.*, 2018, **117**, 1–14.
73 A. A. Lee, Y. S. Chen, E. Ekalestari, S. Ho, N. Hsu, T. Kuo and T. A. Wang, *Angew. Chem., Int. Ed. Engl.*, 2016, **55**, 12338–12342.

© 2021 The Author(s). Published by the Royal Society of Chemistry

Open Access Article. Published on 17 June 2021. Downloaded on 10/3/2024 11:52:16 PM. This article is licensed under a Creative Commons Attribution-NonCommercial 3.0 Unported Licence.

74 M. B. Nodwell and R. Britton, *ACS Infect. Dis.*, 2020, **7**, 153–161.
75 A. Sargun, T. C. Johnstone, H. Zhi, M. Raffatellu and E. Nolan, *Chem. Sci.*, 2021, **12**, 4041–4056.
76 K. Ferreira, H. Y. Hu, V. Fetz, H. Prochnow, B. Rais, P. P. Müller and M. Brönstrup, *Angew. Chem., Int. Ed.*, 2017, **56**, 8272–8276.
77 M. Schnabelrauch, S. Wittmann, K. Rahn, U. Möllmann, R. Reissbrodt and L. Heinisch, *BioMetals*, 2000, **13**, 333–348.
78 C. Y. Zamora, A. G. E. Madec, W. Neumann, E. M. Nolan and B. Imperiali, *Bioorg. Med. Chem.*, 2018, **26**, 5314–5321.
79 S. K. Buchanan, B. S. Smith, L. Venkatramani, D. Xia, L. Esser, M. Palnitkar, R. Chakraborty, D. Van Der Helm and J. Deisenhofer, *Nat. Struct. Biol.*, 1999, **6**, 56–63.
80 W. Rabsch, W. Voigt, R. Reissbrodt, R. M. Tsolis and A. J. Bäumler, *J. Bacteriol.*, 1999, **181**, 3610–3612.
81 K. Hantke, G. Nicholson, W. Rabsch and G. Winkelmann, *Proc. Natl. Acad. Sci. U. S. A.*, 2003, **100**, 3677–3682.
82 T. A. Russo, C. D. McFadden, U. B. Carlino-MacDonald, J. M. Beanan, T. J. Barnard and J. R. Johnson, *Infect. Immun.*, 2002, **70**, 7156–7160.
83 T. C. Johnstone and E. M. Nolan, *J. Am. Chem. Soc.*, 2017, **139**, 15245–15250.
84 F. Peuckert, M. Miethke, A. G. Albrecht, L. O. Essen and M. A. Marahiel, *Angew. Chem., Int. Ed.*, 2009, **48**, 7924–7927.
85 F. Peuckert, A. L. Ramos-Vega, M. Miethke, C. J. Schwörer, A. G. Albrecht, M. Oberthür and M. A. Marahiel, *Chem. Biol.*, 2011, **18**, 907–919.
86 X. Liu, Q. Du, Z. Wang, S. Liu, N. Li, Y. Chen, C. Zhu, D. Zhu, T. Wei, Y. Huang, S. Xu and L. Gu, *FEBS Lett.*, 2012, **586**, 1240–1244.
87 R. J. Abergel, A. M. Zawadzka, T. M. Hoette and K. N. Raymond, *J. Am. Chem. Soc.*, 2009, **131**, 12682–12692.
88 A. Shanzer, J. Libman, S. Lifson and C. E. Felder, *J. Am. Chem. Soc.*, 1986, **108**, 7609–7619.
89 A. Shanzer and J. Libman, *J. Chem. Soc., Chem. Commun.*, 1983, 846–847.
90 R. J. A. Ramirez, L. Karamanukyan, S. Ortiz and C. G. Gutierrez, *Tetrahedron Lett.*, 1997, **38**, 749–752.
91 M. Meyer, J. R. Telford, S. M. Cohen, D. J. White, J. Xu, K. N. Raymond and R. V March, *J. Am. Chem. Soc.*, 1997, **119**, 10093–10103.
92 E. J. Corey and S. Bhattacharyya, *Tetrahedron Lett.*, 1977, 3919–3922.
93 W. H. Rastetter, T. J. Erickson and M. C. Venuti, *J. Org. Chem.*, 1981, **45**, 3579–3590.
94 H. J. Rogers, *J. Chem. Soc., Perkin Trans. 1*, 1995, 3073–3075.
95 T. Baramov, B. Schmid, H. Ryu, J. Jeong, K. Keijzer, L. von Eckardstein, M. H. Baik and R. D. Süssmuth, *Chem.–Eur. J.*, 2019, **25**, 6955–6962.
96 K. Brandhorst and J. Grunenberg, *J. Chem. Phys.*, 2010, **132**, 184101.
97 M. D. Walter, J. Grunenberg and P. S. White, *Chem. Sci.*, 2011, **2**, 2120–2130.
98 J. Grunenberg and N. Goldberg, *J. Am. Chem. Soc.*, 2000, **122**, 6045–6047.
99 J. Grunenberg, *Chem. Sci.*, 2015, **6**, 4086–4088.
100 J. Grunenberg, *Angew. Chem.*, 2017, **129**, 7394–7397.
101 S. S. Isied, G. Kuo and K. N. Raymond, *J. Am. Chem. Soc.*, 1976, **98**, 1763–1767.
102 A. Avdeef, S. R. Sofen, T. L. Bregante and K. N. Raymond, *J. Am. Chem. Soc.*, 1978, **100**, 5362–5370.
103 J. A. Dale, D. L. Dull and H. S. Mosher, *J. Org. Chem.*, 1969, **34**, 2543–2549.
104 K. C. Nicolaou, A. A. Estrada, M. Zak, S. H. Lee and B. S. Safina, *Angew. Chem., Int. Ed.*, 2005, **44**, 1378–1382.
105 I. Shiina, R. Ibuka and M. Kubota, *Chem. Lett.*, 2002, 286–287.
106 J. Inanaga, K. Hirata, H. Saeki, T. Katsuki and M. Yamaguchi, *Bull. Chem. Soc. Jpn.*, 1979, **52**, 1989–1993.
107 H. Gerlach and A. Thalmann, *Helv. Chim. Acta*, 1974, **57**, 2661–2663.
108 E. J. Corey and K. C. Nicolaou, *J. Am. Chem. Soc.*, 1974, **96**, 5614–5616.
109 U. Möllmann, L. Heinisch, A. Bauernfeind, T. Köhler and D. Ankel-Fuchs, *BioMetals*, 2009, **22**, 615–624.
110 N. Ohi, B. Aoki, T. Kuroki, M. Matsumoto, K. Kojima and T. Nehashi, *J. Antibiot.*, 1987, **40**, 22–28.
111 N. Sukhbaatar and T. Weichhart, *Pharmaceuticals*, 2018, **11**, 137.
112 T. Ganz, *Int. J. Hematol.*, 2018, **107**, 7–15.
113 Q. Perraud, P. Cantero, B. Roche and V. Gasser, *Mol. Cell. Proteomics*, 2020, **19**, 589–607.
114 P. Aisen and I. Listowsky, *Annu. Rev. Biochem.*, 1980, **49**, 357–393.
115 J. B. Neilands and K. Konopka, *Biochemistry*, 1984, **23**, 2122–2127.

© 2021 The Author(s). Published by the Royal Society of Chemistry